Unit-cell parameters for scapolite solid solutions and a discontinuity at Me_{75}, ideally $NaCa_3[Al_5Si_7O_{24}](CO_3)$

Sytle M. Antao[a)]
Department of Geoscience, University of Calgary, Calgary, Alberta T2N 1N4, Canada

(Received 29 March 2013; accepted 22 July 2013)

Twenty-seven scapolite samples from various localities and with compositions between $Me_{6–93}$ were obtained using electron microprobe analysis (EMPA). Their unit-cell parameters were obtained using synchrotron high-resolution powder X-ray diffraction (HRPXRD) data and Rietveld structure refinements using space group $P4_2/n$. The EMPA data show the well-known discontinuity at Me_{75}. In addition, the unit-cell parameters, especially c, show a discontinuity at Me_{75} (=five Al atoms per formula unit, *apfu*), ideally $NaCa_3[Al_5Si_7O_{24}](CO_3)$, where the scapolite solid solution is divided into two ($Me\% = [Ca/(Ca + Na + K)] \times 100$). A maximum c parameter value occurs at $Me_{37.5}$ (=four Al *apfu* ideally), where complete Al–Si, Na–Ca, and Cl–CO_3 order occurs. The unit-cell volume, V, varies smoothly with $Me\%$ and Al *apfu* across the series. © *2013 International Centre for Diffraction Data.* [doi:10.1017/S0885715613000638]

Key words: Scapolite, solid solutions, unit-cell parameters, HRPXRD, end-member Me_{75}, Rietveld refinement, crystal structure

I. INTRODUCTION

Scapolite is the name of a group of volatile-bearing framework aluminosilicate minerals, $(Na,Ca,K)_4[(Al,Si)_3Al_3Si_6O_{24}](Cl,CO_3,SO_4)$, that occur in a variety of metamorphic and igneous rocks. They exhibit compositional and structural complexities. Scapolites store volatiles in the lower crust and upper mantle (Lovering and White, 1969), and are indicators of the activities of the volatile components (Moecher and Essene, 1990, 1991; Jiang *et al.*, 1994; Kullerud and Erambert, 1999). The volatile components in scapolite indicate that they may play a natural role in the capture and storage of greenhouse gases.

Ideal solid solutions between end members in a binary system generally give rise to simple relations between structural parameters, including unit-cell parameters and chemical compositions. Hitherto, no simple relation is observed for scapolite solid solutions because of antiphase domain boundaries (APBs), Ca–Na, Cl–CO_3, and Al–Si order across the series. Nevertheless, scapolite-group minerals are excellent materials to investigate the relations between compositional and structural parameters. The tetragonal unit-cell parameters for scapolite are independent of the space group chosen (either $I4/m$ or $P4_2/n$).

In this study, based on 27 samples across the scapolite series, electron microprobe analyses (EMPA), and unit-cell parameters obtained from synchrotron high-resolution powder X-ray diffraction (HRPXRD) and Rietveld structure refinements using space group $P4_2/n$ indicate that there are two series: $Me_{0–75}$ and $Me_{75–100}$ with a discontinuity at Me_{75}. Across the series, the composition is given as $Me\% = [Ca/(Ca + Na + K)] \times 100$. A maximum c value occurs at $Me_{37.5}$, midway between $Me_{0–75}$, where maximum Al–Si, Ca–Na, and Cl–CO_3 order were observed (Hassan and Buseck, 1988; Antao and Hassan, 2011a, 2011b).

Scapolite forms solid solutions between the extreme end-members marialite, $Na_4[Al_3Si_9O_{24}]Cl = Me_0$ and meionite, $Ca_4[Al_6Si_6O_{24}]CO_3 = Me_{100}$ (Deer *et al.*, 1992). A near end-member silvialite, $Ca_4[Al_6Si_6O_{24}]SO_4$, is known (Teertstra *et al.*, 1999). Scapolite forms two series that meet at end-member Me_{75}, $Na_2Ca_6[Al_{10}Si_{14}O_{48}](CO_3)_2$, and the composition varies by replacement of $[Na_4 \cdot Cl]Si_2$ for $[NaCa_3 \cdot CO_3]Al_2$ between $Me_{0–75}$, and by the replacement of $[NaCa_3 \cdot CO_3]Si$ for $[Ca_4 \cdot CO_3]Al$ between $Me_{75–100}$ (Evans *et al.*, 1969; Hassan and Buseck, 1988; Deer *et al.*, 1992). Chemical analyses of scapolite are represented by two straight lines that meet at Me_{75}, indicating two series (see Fig. 12 in Hassan and Buseck, 1988; or Fig. 188 in Deer *et al.*, 1992). The Ca–Na cations disorder on heating, but the Cl–CO_3 order remains at 900 °C (Antao and Hassan, 2002, 2008a, 2008b). The $Me_{37.5}$ (midway between $Me_{0–75}$) composition, $Na_5Ca_3[Al_8Si_{16}O_{48}]Cl(CO_3)$, has a ratio of clusters $[Na_4^{\cdot}Cl]^{3+}$:$[NaCa_3^{\cdot}CO_3]^{5+} = 1:1$, where complete cluster order occurs, and full Al–Si order is expected. $Me_{37.5}$ is where the maximum intensities occur for the type-b ($h + k + l$ = odd) reflections (Lin and Burley, 1973a, 1973b, 1973c; see Fig. 2 in Hassan and Buseck, 1988). The crystal structure of a composition close to $Me_{37.5}$ was obtained by Antao and Hassan (2011a). Complete Al–Si order was observed, and a maximum value occurs for the c parameter.

Some studies divided the scapolite series into three subseries at $Me_{20–25}$ and $Me_{60–67}$ based on discontinuities in the c unit-cell parameter (e.g., Sokolova *et al.*, 1996, 2000; Teertstra and Sherriff, 1996; Zolotarev, 1996; Sherriff *et al.*, 1998, 2000; Teertstra *et al.*, 1999; Zolotarev *et al.*, 2003; Hawthorne and Sokolova, 2008; Sokolova and Hawthorne, 2008). At these two discontinuities, no significant changes occur in the

[a)]Author to whom correspondence should be addressed. Electronic mail: ntao@ucalgary.ca

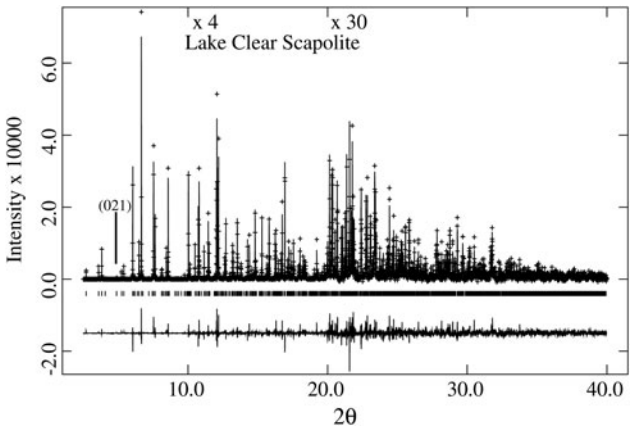

Figure 1. HRPXRD trace for Lake Clear scapolite, $Me_{37.5}$, at 25 °C, together with the calculated (continuous line) and observed (crosses) profiles. The difference curve (I_{obs}–I_{calc}) is shown at the bottom. The short vertical lines indicate allowed reflection positions. The intensities for the trace and difference curve that are above 10° and 20° 2θ are scaled by factors of ×4 and ×30, respectively. The (021) reflection is indicated.

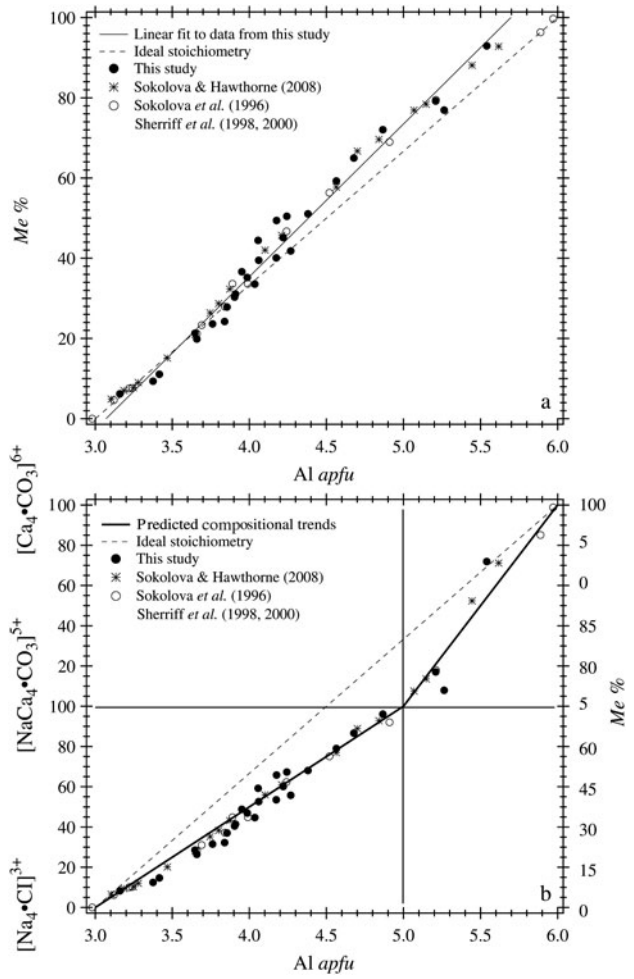

Figure 2. Chemical composition across the scapolite series. (a) The *Me*% increases linearly with Al *apfu*. The least-squares fitted solid line does not pass through the points (Me_0 and Al_3) and (Me_{100} and Al_6) because of scapolite chemical anomaly. (b) Composition shown as two series that meet at (Me_{75} and Al_5) and represented by two thick solid lines that correspond to the ideal theoretical compositions of Me_0, Me_{75}, and Me_{100}. The data points are not fitted in (b). The dashed lines in (a) and (b) represent ideal stoichiometric compositions for scapolite solid solutions that do not occur. Data from the literature are included for comparison (insert).

chemical composition or unit-cell parameters, as observed in this study. The discontinuity in chemical composition at Me_{75} is well-established. One reason for this study is to identify a structural cause for the chemical discontinuity at Me_{75}.

Using transmission electron microscopy (TEM) and the type-*b* reflections that distinguish between the two possible space groups for scapolite, three subseries were identified (Seto *et al.,* 2004). Series $Me_{0–18}$ and $Me_{90–100}$ have space group $I4/m$, and series $Me_{18–90}$ has space group $P4_2/n$. At Me_{18} and Me_{90}, no significant change occurs in composition or unit-cell parameters.

The division of the series into two or three and their boundaries is debatable, and is examined in this study. Where the scapolite series is divided into two that meet at Me_{75}, exchange reactions (given above) show how the composition changes, which is not the case where the series is divided into three. Only at Me_{75}, both the chemical composition and unit-cell parameters consistently show a discontinuity, as is illustrated in this study.

II. EXPERIMENTAL

Twenty-seven scapolite samples between $Me_{6–93}$ from various localities were used in this study (Table I). Their descriptions and compositions were given by Shaw (1960a, 1960b), Evans *et al.* (1969), and Lin and Burley (1973a, 1973b, 1973c) for some samples (Table I). The samples were analyzed using a JEOL JXA-8200 electron microprobe. The JEOL operating program on a Solaris platform was used for ZAF correction and reducing the data. The wavelength-dispersive operating conditions were 15 kV accelerating voltage, 20 nA beam current, and a beam diameter of 5 μm, and used various standards. The crystals are homogeneous based on optical observations and microprobe analyses of eight spots for each sample (≈0.2 mm in diameter). The 27 chemical compositions are given (Table II).

Crystals of scapolite (≈0.2 mm in diameter) were hand-picked under a binocular microscope, and finely crushed in an agate mortar and pestle for synchrotron high-resolution powder X-ray diffraction (HRPXRD) experiments that were performed at beamline 11-BM, Advanced Photon Source, Argonne National Laboratory. Each sample was loaded into a Kapton capillary (0.8 mm internal diameter) and rotated during the experiment at a rate of 90 rotations per second. These data were collected to a maximum 2θ of about 40° with a step size of 0.0005° and a step time of 0.1 s per step. A silicon and alumina NIST standard (ratio of ⅓ Si: ⅔ Al_2O_3 by weight) was used to calibrate the 12-analyzer crystal detector system response, zero offset, and determine the wavelength used in the experiment (see Table I). Additional details of the experimental set-up and data analyses were given (Antao *et al.*, 2008; Lee *et al.*, 2008; Wang *et al.*, 2008).

The unit-cell parameters for the 27 samples were obtained using the Rietveld method (Rietveld, 1969), as implemented in the *GSAS* program (Larson and Von Dreele, 2000), and using the *EXPGUI* interface (Toby, 2001). Structure refinements were conducted by varying parameters in the following sequence: scale factor, background (shifted Chebyschev), cell, zero shift, profile (type-3), atom positions, and isotropic displacement parameters. The chemical composition was used to fix the site occupancies and they were not refined. Finally, all of the other variables were refined simultaneously

https://doi.org/10.1017/S0885715613000638 Published online by Cambridge University Press

TABLE I. Scapolite samples: localities, *Me*%, unit-cell parameters, and *R* (F^2) values.

No.	Code	Locality	*Me*%	*a*	*c*	*V*	*R* (F^2)
1		Badakhshan, Afghanistan	6.2	12.047 56(1)	7.563 21(1)	1097.751(1)	0.0724
2		Badakhshan	9.3	12.054 58(1)	7.567 80(1)	1099.698(1)	0.0741
3		Badakhshan	11.0	12.053 99(1)	7.570 35(1)	1099.962(1)	0.0706
4		Sar-e-Sang, Badakhshan, Afghanistan	19.9	12.056 93(1)	7.575 82(1)	1101.293(1)	0.0734
5		Pamir, Tajikistan	24.2	12.053 29(1)	7.582 16(1)	1101.550(1)	0.0670
6		Gooderham Twp., Ontario	21.3	12.061 61(1)	7.580 77(1)	1102.870(1)	0.0592
7	GL	Gib Lake, Pontiac Twp., Quebec	30.3	12.057 43(1)	7.586 14(1)	1102.885(2)	0.0699
8		Morongoro, Tanzania	23.6	12.066 09(1)	7.580 56(1)	1103.657(2)	0.0870
9a	ON7	Monmouth Twp., Ontario (SXTL)	31.1	12.063 49(1)	7.584 51(1)	1103.756(1)	0.0630
9b	ON7	Monmouth Twp., Ontario (powder)	31.1	12.066 14(1)	7.584 17(1)	1104.193(2)	0.0722
10		Groperto, Brazil	27.8	12.069 09(1)	7.584 11(1)	1104.722(2)	0.0993
11		Madagascar	33.5	12.072 00(1)	7.587 50(1)	1105.752(1)	0.0614
12	CA63A	Grand Calumet, Twp., Quebec	43.9	12.078 16(2)	7.584 02(1)	1106.371(3)	0.0818
13		Lake Clear, Ontario	36.6	12.078 99(1)	7.583 47(1)	1106.443(2)	0.0688
14		Fishtail Lake, Ontario	40.1	12.083 72(1)	7.583 06(1)	1107.250(2)	0.0667
15	ON70	Mpwapwa, Tanzania	40.1	12.085 35(1)	7.582 60(1)	1107.482(1)	0.0635
16	CA30	Grand Calumet Twp., Quebec	35.2	12.084 96(2)	7.583 82(2)	1107.588(4)	0.0529
17		UC17616, unknown	41.8	12.088 29(1)	7.582 50(1)	1108.006(1)	0.0691
18		Otter Lake, Quebec	41.1	12.103 90(1)	7.578 38(1)	1110.267(2)	0.0651
19		Bancroft, Ontario	45.3	12.105 49(1)	7.578 20(1)	1110.531(2)	0.0830
20	Q26	Clapham Twp., Quebec	47.1	12.106 55(1)	7.578 77(1)	1110.809(2)	0.0651
21	Q13	Huddersfield Twp., Quebec	52.3	12.117 15(1)	7.575 64(1)	1112.295(2)	0.0551
22	ON27	Olmsteadville, NY	58.8	12.141 69(1)	7.567 16(1)	1115.554(1)	0.0667
23	Q85	Huddersfield Twp., Quebec	64.1	12.141 72(2)	7.572 58(2)	1116.360(4)	0.0980
24		Blackhills, ND, USA	72.0	12.162 36(1)	7.567 12(1)	1119.351(2)	0.0781
25	ON47	Sluydyanka, Siberia, USSR	79.2	12.165 58(2)	7.574 45(1)	1121.030(3)	0.0795
26		McGill Farm, Quebec	79.6	12.173 09(2)	7.570 64(1)	1121.848(3)	0.1357
27	B20018-1	Mt. Vesuvius, Italy	92.9	12.198 82(1)	7.576 95(1)	1127.535(2)	0.0674

All of the samples were refined in space group $P4_2/n$. 9a was obtained as a large crystal and 9b was obtained as a powdered sample. Monochromatic wavelengths used were 0.402 43(2) Å (samples no.8, 10, 12, 13, 14, 15, 16, and 26); 0.402 41(2) Å (samples no. 7, 9b, 11, 19, 20, and 24); 0.414 17(2) Å (samples no.1 and 26); 0.412 22(2) Å (samples no. 2 and 3), 0.412 204(2) Å (samples no. 4 and 5); 0.412 26(2) Å (samples no. 9a and 17); 0.412 20(2) Å (sample no. 6).

until convergence was achieved. Data for unit-cell and compositional parameters are reported, including the Rietveld *R* (F^2) values (Tables I and II). With these data, equations and correlations factors (R^2) for structural variations can easily be obtained, hence they are not reported. Structural parameters obtained by HRPXRD for a few scapolite samples were reported (Antao and Hassan, 2008a, 2008b, 2011a, 2011b; Antao *et al.*, 2008). As an example, a typical Rietveld fit of a trace is shown in Figure 1 and the following Rietveld statistics were obtained [*R* (F^2) = 0.0688, wR_p (fitted) = 0.0710, $\chi^2 = 2.338$, $N_{obs} = 2959$, 2θ range = 2.5–40°, and $\lambda = 0.402$ 43(2)].

III. RESULTS AND DISCUSSION

The chemical analyses for 27 samples are plotted (Figure 2). The dashed lines indicate the ideal stoichiometry for scapolite, which is not achieved, and is often referred to as scapolite chemical anomaly. The *Me*% increases linearly with Al *apfu* [Figure 2(a)]. Figure 2(b) shows the variation of scapolite analyses as two series that meet at Me_{75}. The thick solid lines are based on the ideal chemical compositions for Me_0, Me_{75}, and Me_{100}, and the measured data points are not fitted [Figure 2(b)]. This variation is the same as that reported by Hassan and Buseck (1988) and shown as Fig. 188 in Deer *et al.* (1992), based on chemical analyses available at that time.

Included for comparison in Figure 2 are data from Sokolova and Hawthorne (2008), Sokolova *et al.* (1996), and Sherriff *et al.* (1998, 2000). The chemical analyses from these studies and the data from this study are similar to each other. The solid straight line passes through the point (Me_0, 3 Al), but does not pass through the (Me_{100}, 6 Al) point [Figure 2(a)]. Compositions above Me_{93} or below Me_6 do not occur naturally; so the synthetic end-members, Me_0 and Me_{100}, are shown.

Based on the chemical analyses, there is only one discontinuity at Me_{75} [or five Al *apfu*; Figure 2(b)]; no other discontinuities occur at any other points such as: $Me_{20–25}$ and $Me_{60–67}$, or Me_{18} and Me_{90}, as were reported in the literature (see Introduction). Can the Me_{75} discontinuity be observed in the unit-cell parameters?

The unit-cell parameters for the 27 scapolite samples may be plotted against *Me*%, Al *apfu*, or *V*. These plots show similar features, irrespective of the variable chosen (Figure 3), three plots are discussed in detail. The *a* and *c* unit-cell parameters show discontinuities at 1120 Å^3 [Figures 3(a) and 3(d)], which corresponds to Me_{75} [=five Al *apfu*; Figures 3(c) and 3(f)]. A maximum in the *c* value occurs at about 1106.5 Å^3, near $Me_{37.5}$ [Figure 3(d)] [=four Al *apfu*; Figure 3(f)]. The data points were fitted by least-squares and are shown as solid quadratic curves or straight lines. It is possible to fit the *c* data points between $Me_{0–75}$ with two straight lines that meet at about $Me_{37.5}$, but a quadratic curve was chosen for the fit over the $Me_{0–75}$ series [Figure 3(d)].

The unit-cell volume, *V*, varies smoothly with *Me*% [Figure 3(j)], and with Al *apfu* [Figure 3(k)]; in both of these cases no discontinuity occurs at Me_{75}. However, it is possible to fit the same *V* data to show a discontinuity at five Al *apfu* [Figure 3(l)]. For a first-order transition, it is important for *V*

https://doi.org/10.1017/S0885715613000638 Published online by Cambridge University Press

TABLE II. Chemical composition and *Me%* for scapolite samples.

Wt. %	1	2	3	4	5	6	7	8a	9	10	11	12	13	14
SiO_2	62.67	60.27	60.07	58.28	56.79	57.86	54.91	56.92	55.15	55.46	53.97	52.04	54.72	53.58
Al_2O_3	19.00	20.01	20.29	21.69	22.66	21.43	22.46	22.04	22.63	22.28	23.19	22.55	22.79	23.24
FeO	0.02	0.04	0.04	0.00	0.06	0.00	0.31	0.10	0.03	0.12	0.05	0.10	0.08	0.19
SrO	0.00	0.00	0.00	0.00	0.00	0.04	0.00	0.00	0.00	0.00	0.00	0.00	0.20	0.00
MgO	0.00	0.00	0.00	0.00	0.01	0.00	0.05	0.00	0.04	0.02	0.00	0.09	0.00	0.02
CaO	1.57	2.38	2.84	4.92	5.99	5.47	7.49	5.87	7.77	6.84	8.12	11.05	8.58	9.85
Na_2O	12.31	11.74	11.61	10.15	9.89	10.39	9.03	9.53	8.95	8.83	8.08	7.20	7.67	7.34
K_2O	1.32	1.59	1.52	1.25	0.73	1.16	0.74	1.50	0.85	1.46	1.27	0.93	0.84	1.22
Cl	3.50	3.49	3.48	3.07	2.87	3.09	2.53	2.86	2.73	2.59	2.54	1.60	2.21	1.80
SO_3	0.14	0.11	0.10	0.13	0.35	0.03	0.68	0.47	0.33	0.78	0.30	0.60	0.37	1.30
CO_2	0.76	0.72	0.75	1.24	1.35	1.22	1.46	1.26	1.42	1.34	1.65	2.48	2.04	1.99
–O = Cl	0.80	0.80	0.80	0.70	0.66	0.71	0.58	0.65	0.62	0.59	0.58	0.37	0.50	0.41
Total	100.49	99.55	99.89	100.02	100.04	99.98	99.06	99.88	99.27	99.12	98.58	98.28	98.98	100.13
apfu														
Si	8.841	8.625	8.583	8.341	8.162	8.353	8.097	8.240	8.089	8.144	7.966	7.943	8.050	7.940
Al	3.159	3.375	3.417	3.659	3.838	3.647	3.903	3.760	3.911	3.856	4.034	4.057	3.950	4.060
ΣT	12.00	12.00	12.00	12.00	12.00	12.00	12.00	12.00	12.00	12.00	12.00	12.00	12.00	12.00
Fe^{2+}	0.002	0.005	0.004	0.000	0.008	0.000	0.038	0.012	0.004	0.015	0.007	0.013	0.010	0.023
Sr	0.000	0.000	0.000	0.000	0.000	0.003	0.000	0.000	0.000	0.000	0.000	0.000	0.017	0.000
Mg	0.000	0.000	0.000	0.000	0.001	0.000	0.011	0.000	0.008	0.005	0.000	0.020	0.000	0.005
Ca	0.238	0.365	0.434	0.755	0.923	0.847	1.183	0.910	1.221	1.075	1.284	1.807	1.352	1.564
Na	3.366	3.258	3.217	2.816	2.755	2.907	2.581	2.673	2.545	2.513	2.311	2.131	2.186	2.108
K	0.238	0.290	0.277	0.227	0.134	0.213	0.139	0.276	0.158	0.273	0.238	0.181	0.158	0.230
ΣM	3.844	3.917	3.932	3.798	3.821	3.971	3.952	3.872	3.936	3.882	3.840	4.152	3.724	3.930
Cl	0.838	0.846	0.844	0.744	0.698	0.757	0.632	0.701	0.678	0.645	0.635	0.414	0.550	0.452
(SO_4)	0.015	0.012	0.011	0.013	0.037	0.003	0.075	0.051	0.037	0.086	0.033	0.069	0.040	0.145
(CO_3)	0.147	0.142	0.146	0.242	0.265	0.240	0.293	0.248	0.285	0.269	0.332	0.517	0.409	0.403
ΣA	1.000	1.000	1.000	1.000	1.000	1.000	1.000	1.000	1.000	1.000	1.000	1.000	1.000	1.000
Me%	6.2	9.3	11.0	19.9	24.2	21.3	30.3	23.6	31.1	27.8	33.5	43.9	36.6	40.1

Wt. %	15	16	17	18	19	20	21	22	23	24	25	26	27
SiO_2	52.63	55.17	53.35	52.62	52.73	51.67	51.03	48.98	48.16	45.89	44.05	44.35	41.51
Al_2O_3	23.83	23.28	25.00	23.85	24.27	23.98	24.89	25.51	26.10	26.56	28.67	29.40	30.20
FeO	0.08	0.01	0.06	0.03	0.02	0.16	0.03	0.25	0.02	0.03	0.08	0.00	0.09
SrO	0.11	0.00	0.08	0.00	0.00	0.00	0.00	0.00	0.00	0.05	0.19	0.00	0.08
MgO	0.00	0.00	0.00	0.00	0.02	0.02	0.00	0.08	0.06	0.00	0.07	0.04	0.08
CaO	9.85	8.85	10.39	9.84	11.01	11.30	12.60	14.11	15.54	17.25	18.65	18.69	22.56
Na_2O	7.57	8.94	7.45	7.18	6.73	6.30	5.68	4.63	4.60	3.62	2.55	2.81	0.95
K_2O	0.86	0.11	0.82	0.91	0.95	1.07	1.00	1.27	0.33	0.12	0.24	0.45	0.01
Cl	1.83	2.20	1.74	1.91	1.79	1.75	1.46	1.03	0.71	0.39	0.03	1.03	0.19
SO_3	1.02	0.21	1.14	0.80	1.36	1.08	1.37	0.02	1.60	0.00	1.63	1.17	0.17
CO_2	2.10	2.19	2.27	2.11	2.00	2.11	2.34	3.54	3.06	4.23	3.20	2.90	4.38
–O = Cl	0.42	0.50	0.40	0.44	0.41	0.40	0.33	0.24	0.16	0.09	0.01	0.24	0.04
Total	99.46	100.44	101.89	98.81	100.46	99.04	100.06	99.18	100.02	98.04	99.35	100.59	100.17
apfu													
Si	7.825	8.015	7.731	7.823	7.780	7.757	7.620	7.436	7.322	7.134	6.791	6.737	6.460
Al	4.175	3.985	4.269	4.177	4.220	4.243	4.380	4.564	4.678	4.866	5.209	5.263	5.540
ΣT	12.00	12.00	12.00	12.00	12.00	12.00	12.00	12.00	12.00	12.00	12.00	12.00	12.00
Fe^{2+}	0.010	0.001	0.008	0.003	0.002	0.020	0.003	0.032	0.003	0.003	0.010	0.000	0.012
Sr	0.010	0.000	0.007	0.000	0.000	0.000	0.000	0.000	0.000	0.005	0.017	0.000	0.007
Mg	0.000	0.000	0.000	0.000	0.003	0.004	0.000	0.018	0.014	0.000	0.016	0.008	0.018
Ca	1.569	1.377	1.613	1.567	1.741	1.818	2.015	2.295	2.532	2.873	3.081	3.043	3.762
Na	2.183	2.517	2.094	2.068	1.924	1.834	1.644	1.363	1.356	1.092	0.762	0.827	0.287
K	0.163	0.020	0.152	0.173	0.178	0.205	0.191	0.246	0.063	0.024	0.047	0.087	0.001
ΣM	3.935	3.915	3.873	3.811	3.848	3.881	3.854	3.954	3.967	3.997	3.933	3.965	4.087
Cl	0.461	0.542	0.428	0.482	0.447	0.445	0.368	0.265	0.183	0.102	0.008	0.265	0.050
(SO_4)	0.114	0.023	0.124	0.089	0.151	0.122	0.154	0.002	0.183	0.000	0.189	0.133	0.020
(CO_3)	0.425	0.435	0.449	0.429	0.402	0.433	0.478	0.733	0.635	0.898	0.804	0.602	0.930
ΣA	1.000	1.000	1.000	1.000	1.000	1.000	1.000	1.000	1.000	1.000	1.000	1.000	1.000
Me%	40.1	35.2	41.8	41.1	45.3	47.1	52.3	58.8	64.1	72.0	79.2	76.9	92.9

Me% = [Ca/(Ca + Na + K)] × 100; Analyses 11, 19, 21, and 24 are taken from Evans *et al.* (1969) as the samples were used up. CO_2 was calculated from stoichiometry assuming ΣA = 1. The *apfu* were calculated based on Si + Al = 12.

https://doi.org/10.1017/S0885715613000638 Published online by Cambridge University Press

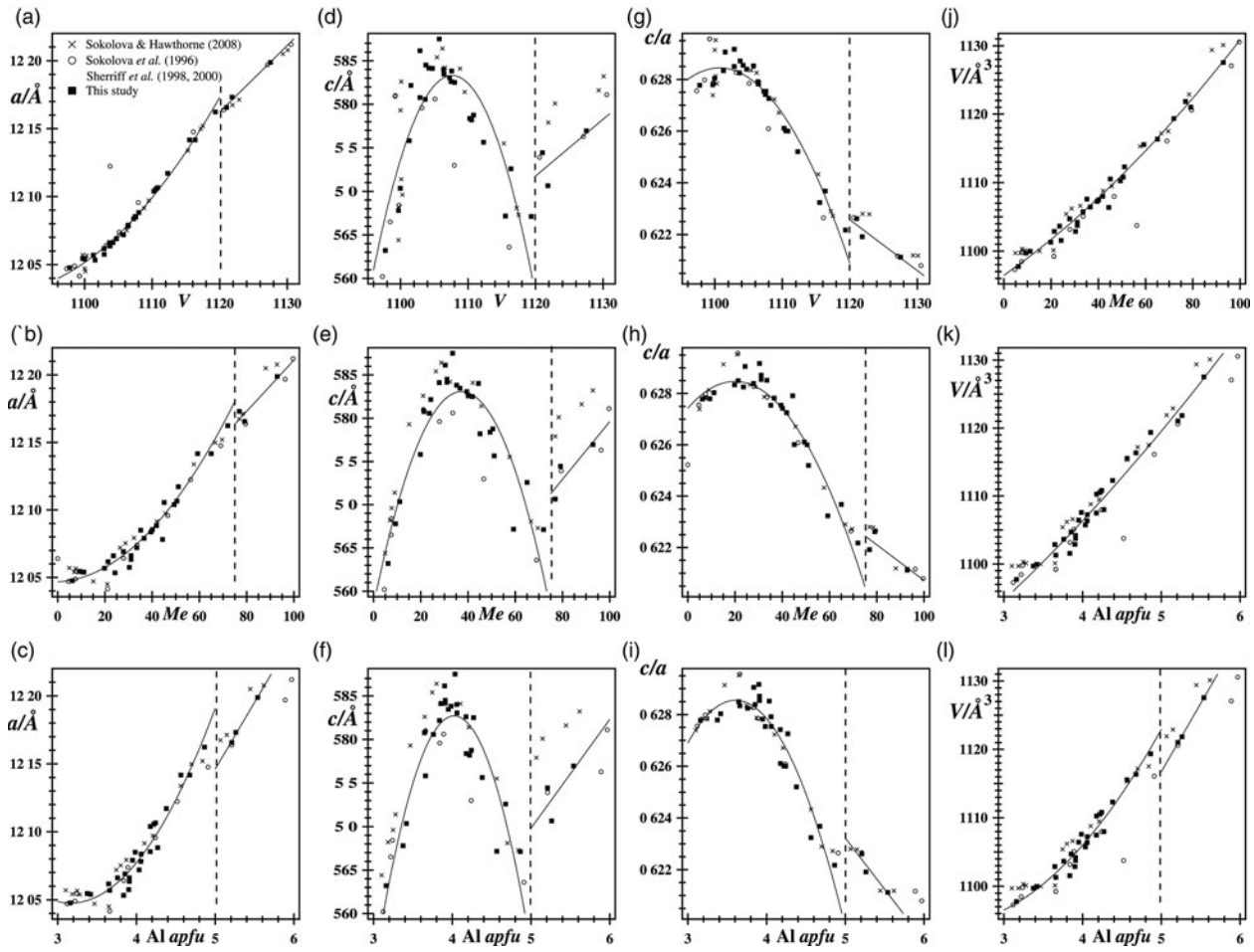

Figure 3. Variation of the unit-cell parameters across the scapolite series. (a) *a* vs. *V*, (b) *a* vs. *Me*%, (c) *a* vs. Al *apfu*, (d) *c* vs. *V*, (e) *c* vs. *Me*%, (f) *c* vs. Al *apfu*, (g) c/*a* vs. *V*, (h) c/*a* vs. *Me*%, (i) c/*a* vs. Al *apfu*, (j) *V* vs. *Me*%, (k) *V* vs. Al *apfu*, and (l) *V* vs. Al *apfu*. A dashed vertical line is drawn at 1120 Å^3, Me_{75}, and five Al *apfu* where a discontinuity occurs. A maximum *c* value occurs at $Me_{37.5}$, and four Al *apfu* (d, e, and f). A continuous non-linear variation is shown for *V* vs. *Me* % or Al *apfu* (j and k), which rules out any phase transition in the scapolite series.

to show a significant change, instead of changes in the *a* or *c* unit-cell parameters. Such a transition would also require additional confirmation, such as a change in space group at that particular point. Since the *V* does not show a discontinuity between $Me_{0–100}$ [Figures 3(j) and 3(k)], no first-order transition occurs in the scapolite series, but a second-order transition at Me_{75} cannot be ruled out. Therefore, point Me_{75} is considered as a discontinuity instead of a transition.

There is no 1:1 correspondence between *V*, *Me*%, and Al *apfu* because the dashed vertical lines should occur at the same position on the horizontal *x*-axis (Figure 3). For example, the dashed vertical line at Me_{75} occurs to the right of similar lines for *V* or Al *apfu* [Figures 3(a)–3(c)]. The *V* and Al *apfu* have a closer 1:1 correspondence than *Me*% [Figures 3(a) and 3(c)]. One expects the Me_{75} vertical line to coincide with the dashed vertical line at five Al *apfu* based on the Me_{75} formula, $NaCa_3[Al_5Si_7O_{24}](CO_3)$; which is not the case [Figures 3(b) and 3(c)].

The net change in the *c* value between $Me_{0–100}$ is small; about 7.556–7.588 Å, a difference of 0.032 Å, which corresponds to 0.42%. The net change in the *a* parameter is large; about 12.033–12.232 Å, a difference of 0.199 Å, which corresponds to 1.65%, and is about six times larger than the change in *c* value. Large changes are measured more accurately than small changes. The present data and those of Sokolova and Hawthorne (2008) agree quite well for the *a* parameter [Figure 3(a)], but they disagree for the *c* parameter near the end members [Figure 3(d)]. The largest differences between these datasets are seen between $Me_{75–100}$, where two samples (25 and 27 in Table I) were used in many studies. The data shown as open circles were obtained by Rietveld refinements and are closer to the values from this study than to those obtained from the single-crystal method [Figure 3(d)]. Unit-cell parameters obtained by the Rietveld method, especially with HRPXRD data, are typically more accurate than those obtained by the single-crystal method.

Unit-cell parameters are generally measured more accurately than chemical compositions, so when *a*, *c*, and *c*/*a* are plotted against *V* from different studies, they are closer to each other [Figures 3(a), 3(d) and 3(g)], but they are more spread out when they are plotted against compositions such as *Me*% or Al *apfu* (Figure 3).

Based on the *c* unit-cell parameter, a number of studies divided the scapolite series into three subseries with transitions at $Me_{20–25}$ and $Me_{60–67}$, but not at Me_{75}. These data are included for comparison in the figures shown for this study, and all of the data appear to support the discontinuity at Me_{75}. Between $Me_{75–100}$, the cell parameters are slightly different among various studies, but they fall on similar parallel trend lines [Figures 3(a) and 3(d)]. The present data do not support a transition at $Me_{60–67}$.

https://doi.org/10.1017/S0885715613000638 Published online by Cambridge University Press

The data from Sokolova and Hawthorne (2008) occur as a cluster of six points between $Me_{0–21}$, which may indicate a separate trend and a transition at $Me_{20–25}$, as they have reported (Figure 3). These six data points occur on a nearly vertical straight line, indicating that they are independent of *V* [Figures 3(a) and 3(d)], but they do vary with *Me*% (and Al *apfu*), which is unusual [Figure 3(j)]; the *V* for these six points is constant between $Me_{0–21}$. Hawthorne and Sokolova (2008) suggested introduction of K atoms into the structure as a cause for the transition at $Me_{20–25}$. The data from this study indicate that a transition at $Me_{20–25}$ is unlikely (Figure 3). The large K atom should cause a significant change in *V*, which is not observed (Figure 3).

The normalized unit-cell parameters are shown in Figure 4. Both V/V_0 and a/a_0 vary linearly with *Me*% and show no discontinuity. The a_0, c_0, and V_0 values used are 12.047 56(1), 7.563 21(1), and 1097.751(1) Å, respectively, for sample-1 (Table I). The non-linear variation of c/c_0 shows a maximum value at about $Me_{37.5}$ and a minimum value at about Me_{75} (Figure 4).

Some studies did not report a discontinuity at Me_{75} and appear to incorrectly identify phase transitions in the ranges $Me_{20–25}$ and $Me_{60–67}$ (Sokolova *et al.*, 1996; Teertstra and Sherriff, 1996, 1997; Zolotarev, 1996; Sherriff *et al.*, 1998, 2000; Sokolova and Hawthorne, 2008). In this study, a discontinuity occurs at Me_{75} (=five Al *apfu*), and a maximum *c* value occurs at $Me_{37.5}$ (=four Al *apfu*). Maximum order of Al–Si, Cl–CO_3, and Na–Ca, together with APBs occur at $Me_{37.5}$ (Hassan and Buseck, 1988; Antao and Hassan, 2011a).

Why do the *c* values show some scatter between 1103 and 1108 Å^3, that is, near $Me_{37.5}$ [Figure 3(d)]? This scatter is related to APBs and the averaging of different domains containing different clusters that form with Cl and CO_3 ions, including minor SO_4^{2-} and K^+ ions, and the different percentages of such clusters.

Unit-cell data across the scapolite series, particularly the *c* parameter, contain a discontinuity at Me_{75}, $Na_2Ca_6[Al_{10}Si_{14}O_{48}](CO_3)_2$, which does not correspond to a first-order

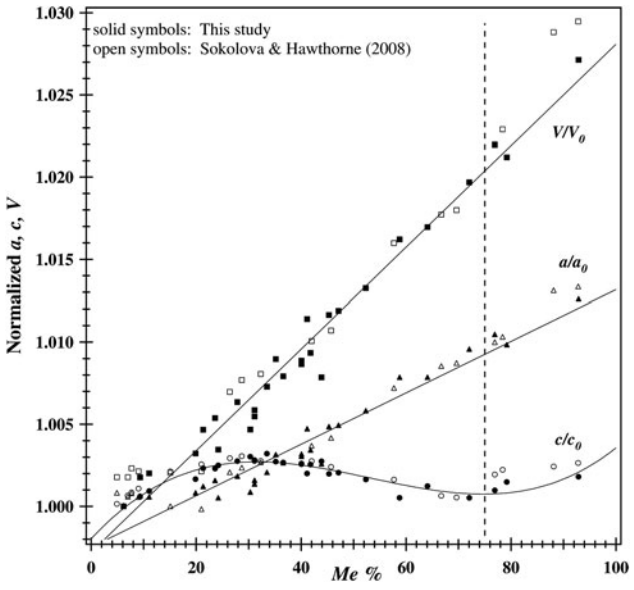

Figure 4. Normalized unit-cell parameters. Both V/V_0 and a/a_0 vary linearly with *Me*%. The non-linear variation of c/c_0 shows a maximum value at about $Me_{37.5}$ and a minimum value at about Me_{75}.

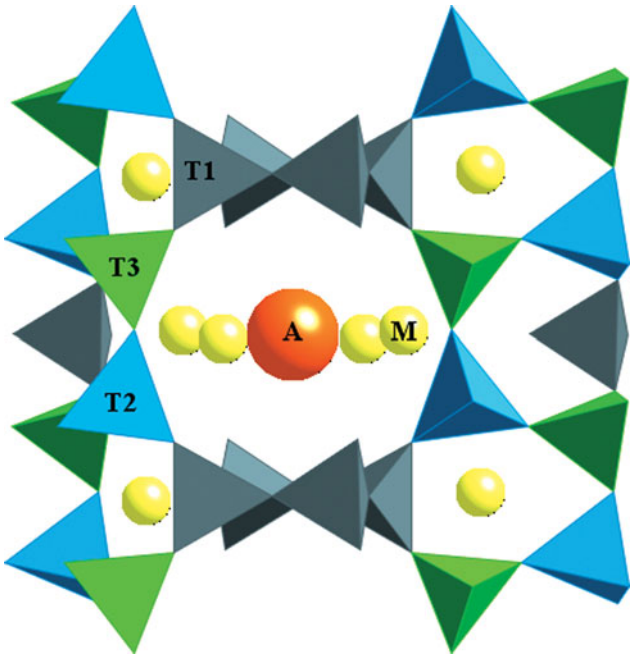

Figure 5. (Color online) Part of the structure of scapolite showing a central cage containing the interstitial framework M cations and A anions and a few five-membered rings in space group $P4_2/n$. The *c* unit-cell parameter is related to the Al–Si order in the T sites and a maximum *c* value occurs at $Me_{37.5}$ (=four Al *apfu*) where complete Al–Si order is shown (T1 and T3 = Si, and T2 = Al; Antao and Hassan, 2011a).

transition; it marks the point where the series is divided into two with distinct exchange reactions (Evans *et al.*, 1969; Hassan and Buseck, 1988). Note that type-*b* reflections were observed between $Me_{18–90}$ (Seto *et al.*, 2004). At Me_{75}, the A site ideally contains only CO_3 groups and no Cl atoms.

A detailed explanation of the unit-cell variations across the scapolite series with composition must come from bond distances and angles and will be addressed in a separate paper, but a qualitative explanation is given here. The height of a TO_4 tetrahedron is about 2.5 Å, and the height of three tetrahedra is 7.5 Å, which is similar to the *c* parameter value in scapolite (Table I; Figure 5). The variation in the *c* parameter across the series is related to the Al–Si order. A maximum *c* value occurs where there is complete Al–Si order at $Me_{37.5}$ (Antao and Hassan, 2011a). From $Me_{0–100}$, Al replaces Si [Al–O > Si-O], larger CO_3 group replaces Cl, longer *M* (Ca, Na site) –*A* (Cl, CO_3 site) distances occur, hence *a* and *V* increase. This increase in *a* and *V* is restrained by stronger <Ca–O> bonds that decrease and cause the TO_4 tetrahedra to rotate, resulting in decreasing T–O–T angles, as Ca replaces Na from $Me_{0–100}$.

Scapolite forms two solid solutions that meet at Me_{75}, $Na_2Ca_6[Al_{10}Si_{14}O_{48}](CO_3)_2$, where a discontinuity occurs in the unit-cell parameters and chemical compositions. Division of the scapolite series into two at Me_{75} was as previously observed (Evans *et al.*, 1969; Hassan and Buseck, 1988). Me_{75} is a valid end-member.

ACKNOWLEDGEMENTS

The author would like to thank late D. M. Shaw and J. Post for providing some scapolite samples. The author also thanks the two anonymous reviewers for their comments. Use of the Advanced Photon Source was supported by the US

https://doi.org/10.1017/S0885715613000638 Published online by Cambridge University Press

Department of Energy, Office of Science, Office of Basic Energy Sciences, under Contract no. DE-AC02-06CH11357. This work was supported by a Discovery grant from the National Science and Engineering Research Council of Canada and an Alberta Ingenuity New Faculty Award.

Antao, S. M. and Hassan, I. (**2002**). "Thermal behavior of scapolite $Me_{79.6}$ and $Me_{33.3}$," Can. Mineral. **40**, 1395–1401.

Antao, S. M. and Hassan, I. (**2011a**). "Complete Al-Si order in scapolite $Me_{37.5}$, ideally $Ca_3Na_5[Al_8Si_{16}O_{48}]Cl(CO_3)$, and implications for anti-phase domain boundaries (APBs)," Can. Mineral. **49**, 581–586.

Antao, S. M. and Hassan, I. (**2011b**). "The structures of marialite (Me_6) and meionite (Me_{93}) in space groups $P4_2/n$ and $I4/m$, and the absence of phase transitions in the scapolite series," Powder Diffr. (USA) **26**, 119–125.

Antao, S. M. and Hassan, I. (**2008a**). "Increase in Al-Si and Na-Ca disorder with temperature in scapolite $Me_{32.9}$," Can. Mineral. **46**, 1577–1591.

Antao, S. M. and Hassan, I. (**2008b**). "Unusual Al-Si ordering in calcic scapolite, $Me_{79.6}$, with increasing temperature," Am. Mineral. (USA) **93**, 1470–1477.

Antao, S. M., Hassan, I., Wang, J., Lee, P. L., and Toby, B. H. (**2008**). "State-of-the-art high-resolution powder X-ray diffraction (HRPXRD) illustrated with Rietveld structure refinement of quartz, sodalite, tremolite, and meionite," Can. Mineral. **46**, 1501–1509.

Deer, W. A., Howie, R. A., and Zussman, J. (**1992**). *An Introduction to the Rock-Forming Minerals* (John Wiley, New York, NY), 2nd ed.

Evans, B. W., Shaw, D. M., and Haughton, D. R. (**1969**). "Scapolite stoichiometry," Contrib. Mineral. Petrol. **24**, 293–305.

Hassan, I. and Buseck, P. R. (**1988**). "HRTEM characterization of scapolite solid solutions," Am. Mineral. (USA) **73**, 119–134.

Hawthorne, F. C. and Sokolova, E. (**2008**). "The crystal chemistry of the scapolite-group minerals. II. The origin of the $I4/m \longleftrightarrow P4_2/n$ phase transition and the nonlinear variations in chemical composition," Can. Mineral. **46**, 1555–1575.

Jiang, S. Y., Palmer, M. R., Xue, C. J., and Li, Y. H. (**1994**). "Halogen-rich scapolite-biotite rocks from the Tongmugou Pb-Zn deposit, Qinling, north-western China: implications for the ore-forming process," Mineral. Mag. **58**, 543–552.

Kullerud, K. and Erambert, M. (**1999**). "Cl-scapolite, Cl-amphibole, and plagioclase equilibria in ductile shear zones at Nusfjord, Lofoten, Norway: implications for fluid compositional evolution during fluid-mineral interaction in the deep crust," Geochim. Cosmochim. Acta **63**, 3829–3844.

Larson, A. C. and Von Dreele, R. B. (**2000**). *General Structure Analysis System (GSAS)*. Report, LAUR 86–748. Los Alamos National Laboratory.

Lee, P. L., Shu, D., Ramanathan, M., Preissner, C., Wang, J., Beno, M. A., Von Dreele, R. B., Ribaud, L., Kurtz, C., Antao, S. M., Jiao, X., and Toby, B. H. (**2008**). "A twelve-analyzer detector system for high-resolution powder diffraction," J. Synchrotron Radiat. (Denmark) **15**, 427–432.

Lin, S. B. and Burley, B. J. (**1973a**). "Crystal structure of a sodium and chlorine-rich scapolite," Acta Crystallogr. **B29**, 1272–1278.

Lin, S. B. and Burley, B. J. (**1973b**). "The crystal structure of meionite," Acta Crystallogr. **B29**, 2024–2026.

Lin, S. B. and Burley, B. J. (**1973c**). "On the weak reflections violating body-centered symmetry in scapolites," Tschermaks Mineralogisch-Petrologische Mitteilungen **20**, 28–44.

Lovering, J. F. and White, A. J. R. (**1969**). "Granulitic and eclogitic inclusions from basic pipes at Delegate, Australia," Contrib. Mineral. Petrol. **21**, 9–52.

Moecher, D. P. and Essene, E. J. (**1990**). "Phase-equilibria for calcic scapolite, and implications of variable Al-Si disorder for *P-T*, T-X_{CO2}, and *a-X* relations," J. Petrol. **31**, 997–1024.

Moecher, D. P. and Essene, E. J. (**1991**). "Calculation of CO_2 activities using scapolite equilibria: constraints on the presence and composition of a fluid phase during high-grade metamorphism," Contrib. Mineral. Petrol. **108**, 219–240.

Rietveld, H. M. (**1969**). "A profile refinement method for nuclear and magnetic structures," J. Appl. Crystallogr. (Denmark) **2**, 65–71.

Seto, Y., Shimobayashi, N., Miyake, A., and Kitamura, M. (**2004**). "Composition and $I4/m$-$P4_2/n$ phase transition in scapolite solid solutions," Am. Mineral. (USA) **89**, 257–265.

Shaw, D. M. (**1960a**). "The geochemistry of scapolite. Part I. Previous work and general mineralogy," J. Petrol. **1**, 218–260.

Shaw, D. M. (**1960b**). "The geochemistry of scapolite. Part II. Trace elements, petrology, and general geochemistry," J. Petrol. **1**, 261–285.

Sherriff, B. L., Sokolova, E. V., Kabalov, Y. K., Teertstra, D., Kunath-Fandrei, G., Goetz, S., and Jäger, C. (**1998**). "Intermediate scapolite: ^{29}Si MAS and ^{27}Al SATRAS NMR spectroscopy and Rietveld structure-refinement," Can. Mineral. **36**, 1267–1283.

Sherriff, B. L., Sokolova, E. V., Kabalov, Y. K., Jenkins, D. M., Kunath-Fandrei, G., Goetz, S., Jäger, C., and Schneider, J. (**2000**). "Meionite: Rietveld structure-refinement, ^{29}Si MAS and ^{27}Al SATRAS NMR spectroscopy, and comments on the marialite-meionite series," Can. Mineral. **38**, 1201–1213.

Sokolova, E. and Hawthorne, F. C. (**2008**). "The crystal chemistry of the scapolite-group minerals. I. Crystal structure and long-range order," Can. Mineral. **46**, 1527–1554.

Sokolova, E. V., Kabalov, Y. K., Sherriff, B. L., Teertstra, D. K., Jenkins, D. M., Kunath-Fandrei, G., Goetz, S., and Jäger, C. (**1996**). "Marialite: Rietveld structure-refinement and ^{29}Si MAS and ^{27}Al satellite transition NMR spectroscopy," Can. Mineral. **34**, 1039–1050.

Sokolova, E. V., Gobechiya, E. R., Zolotarev, A. A., and Kabalov, Y. K. (**2000**). "Refinement of the crystal structures of two marialites from the Kukurt deposit of the east Pamirs," Crystallogr. Rep. **45**, 934–938.

Teertstra, D. K. and Sherriff, B. L. (**1996**). "Scapolite cell-parameter trends along the solid-solution series," Am. Mineral. (USA) **81**, 169–180.

Teertstra, D. K. and Sherriff, B. L. (**1997**). "Substitutional mechanisms, compositional trends and the end-member formulae of scapolite," Chem. Geol. (Isot. Geosci. Sect.) (Netherlands) **136**, 233–260.

Teertstra, D. K., Schindler, M., Sherriff, B. L., and Hawthorne, F. C. (**1999**). "Silvialite, a new sulfate-dominant member of the scapolite group with an Al-Si composition near the $I4/m$-$P4_2/n$ phase transition," Mineral. Mag. **63**, 321–329.

Toby, B. H. (**2001**). "EXPGUI, a graphical user interface for GSAS," J. Appl. Crystallogr. **34**, 210–213.

Wang, J., Toby, B. H., Lee, P. L., Ribaud, L., Antao, S. M., Kurtz, C., Ramanathan, M., Von Dreele, R. B., and Beno, M. A. (**2008**). "A dedicated powder diffraction beamline at the advanced photon source: commissioning and early operational results," Rev. Sci. Instrum. (USA) **79**, 085105.

Zolotarev, A. A. (**1996**). "Once more on isomorphic schemes and isomorphic series in the scapolite group," Zap. Vser. Mineral. Obshchest. **125**, 69–73.

Zolotarev, A. A., Petrov, T. G., and Moshkin, S. V. (**2003**). "Peculiarities of chemical compositions of the scapolite group minerals," Zap. Vser. Mineral. Obshchest. **132**, 63–84.